# Two-dimensional infrared surface spectroscopy for CO on Cu(100): Detection of intermolecular coupling of adsorbates

AUTHOR(S):

Nagata, Y; Tanimura, Y; Mukamel, S

CITATION:

Nagata, Y ...[et al]. Two-dimensional infrared surface spectroscopy for CO on Cu(100): Detection of intermolecular coupling of adsorbates. JOURNAL OF CHEMICAL PHYSICS 2007, 126(20): 204703.

ISSUE DATE:

2007-05-28

URL:

http://hdl.handle.net/2433/49829

THE JOURNAL OF CHEMICAL PHYSICS **126**, 204703 (2007)

# Two-dimensional infrared surface spectroscopy for CO on Cu(100): Detection of intermolecular coupling of adsorbates

Yuki Nagata
*Department of Chemistry, Graduate School of Science, Kyoto University, Sakyo, Kyoto 606-8502, Japan and Department of Chemistry, University of California, Irvine, California 92697-2025*

Yoshitaka Tanimura
*Department of Chemistry, Graduate School of Science, Kyoto University, Sakyo, Kyoto 606-8502, Japan*

Shaul Mukamel
*Department of Chemistry, University of California, Irvine, California 92697-2025*

(Received 11 January 2007; accepted 15 March 2007; published online 23 May 2007; corrected 30 May 2007)

Surface-specific infrared signals obtained by subjecting the system to two infrared laser pulses are calculated for an admixture of CO and isotopic CO on Cu(100) by using molecular dynamics simulation based on a stability matrix formalism. The two-dimensional profiles of the signals in the frequency domain show both diagonal and cross peaks. The former peaks mainly arise from the overtones of the CO and isotopic CO, while the latter represent the couplings between those. As temperature is increased, the phases of cross peaks in a second-order infrared response function change significantly, while those of diagonal peaks are unchanged. The authors show that the phase shifts are originated from the potential anharmonicities due to the electronic interaction between adsorbates. Using a model with two dipole moments, they find that the frustrated rotational mode activated with temperature has effects on the anharmonicity. These results indicate that two-dimensional infrared surface spectroscopy reveals the anharmonic couplings between adsorbates and surface atoms or between adsorbates which cannot be observed in first-order spectroscopy. © *2007 American Institute of Physics*. [DOI: 10.1063/1.2727445]

## I. INTRODUCTION

The vibrational energy dissipation and intermolecular coupling of CO on various metal surfaces have attracted much attention.[1,2] The CO stretching mode lifetime can be explained by an electron-hole (e-h) pair creation mechanism due to the antibonding $2\pi^*$ orbital of the CO molecule.[2] The frustrated CO rotational mode has very short lifetimes dominated by the same mechanism.[3–5] Chemical shifts for the frustrated rotational mode are different for Cu(100) and Cu(111),[6,7] which reflects the sensitivity of the adsorbate dynamics to the electronic structure of metal surfaces due to e-h pair creation. The stretching and frustrated rotational modes are anharmonically coupled to each other.[8,9] At the same time, the CO frustrated rotational and translational modes are coupled.[10] These intermode couplings govern the dynamics of adsorbates on metal surface.

Dipole-dipole interactions play an important role on the geometry and lateral hopping of CO on Pd(100) and Pd(110).[11,12] Researchers have tried to control lateral CO motions.[13–15] The lateral interactions make local ordering of adsorbates and prevent the formation of long range ordered structure at low coverage.[16] Particular attention has been paid to the overtone and combination bands of CO on Ru(001). Broadening of the CO stretch overtone rapidly grows with temperature due to thermally activated decay of two-photon bound state into single phonon states.[17] Large anharmonicities due to lateral couplings lead to the formation of localized two-phonon bound states.[18] Thus, the investigation of the intermolecular couplings of CO adsorbed on metal surface is crucial for revealing the underlying mechanism of the surface dynamics.

In linear spectroscopy the couplings between intra- and interadsorbate interactions are measurable only in terms of chemical shifts. In addition, linear spectroscopy is unable to distinguish homogeneous broadening from inhomogeneous broadening.[19,20] To overcome these limitations, multidimensional spectroscopic techniques have been proposed and carried out to obtain information on surface dynamics. Guyot-Sionnest combined the photon echo and sum-frequency generation (SFG) techniques[21,22] to extract the homogeneous linewidth from the inhomogeneously broadened Si–H vibrations on Si(111) surface.[23] Cho proposed the two-dimensional (2D) infrared-infrared-visible (IR-IR-VIS) SFG[24] and Bonn and co-workers determined the intermolecular coupling strength of dipole-coupled CO on Ru(001) using this SFG.[25,26] However, IR-IR-VIS SFG is a third-order nonlinear optical process and is not surface specific. Belabas and Joffre demonstrated 2D VIS-IR spectroscopy in $AgGaS_2$.[27] Voelkmann *et al.* combined four-wave mixing with the second-harmonic generation to monitor the temporal evolution of photoexcited one- or two-photon coherence.[28]

In this study, we propose to apply 2D IR surface spectroscopy which utilizes the SFG of two independently tunable IR beams to an admixture of $C^{12}O^{16}$ and isotope labeled $C^{13}O^{16}$ on Cu(100). The pulse sequence and energy diagram

 

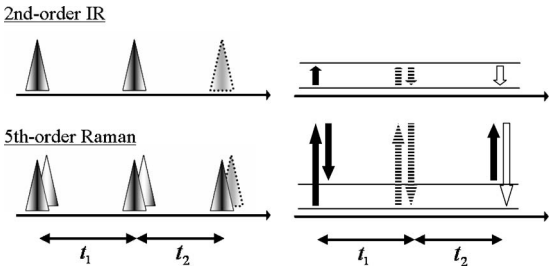


FIG. 1. Pulse sequences (left) and typical energy diagrams (right) for second-order IR surface spectroscopy and fifth-order Raman spectroscopy. Solid and dotted lines denote the transition of bra and ket vectors, respectively.

of 2D IR surface spectroscopy is presented in Fig. 1 with those of 2D Raman spectroscopy. 2D IR surface spectroscopy has two independent time axes retaining the surface specificity and is related to the second-order IR response function

$$R^{(2)}_{abc}(t_2,t_1) = \left(\frac{i}{\hbar}\right)^2 \langle [[\mu_a(t_2),\mu_b(0)],\mu_c(-t_1)]\rangle, \quad (1)$$

where $\mu_q(t)$ is the dipole moment at time $t$ in the $a$ direction.[19,29–31] $t_1$ and $t_2$ are the time intervals between the first and second IR pulses and between the second pulse and the signal, respectively. Since the fifth-order Raman response function

$$R^{(5)}_{abcdef}(t_2,t_1) = \left(\frac{i}{\hbar}\right)^2 \langle [[\Pi_{ab}(t_2),\Pi_{cd}(0)],\Pi_{ef}(-t_1)]\rangle, \quad (2)$$

where $\Pi_{ab}(t)$ is the polarizability at time $t$ in $ab$ tensor, has the same form as the second-order IR response function (1), similar formalisms and simulation strategies developed in 2D Raman spectroscopy[20,32–44] are applicable to 2D IR surface spectroscopy. We calculated 2D IR surface signals by means of molecular dynamics (MD) simulation based on the stability matrix formalism to investigate roles of anharmonic coupling between adsorbates.[33–35,37,40] In third-order IR spectra, $^{13}C$ and $^{18}O$ isotope substitution has been used to change the frequency[45–50] and the cross peaks between two amide-I′ modes were observed.[50] These suggest the possible detection of isotopic effects of adsorbates in 2D IR surface spectroscopy.

The aim of the present article is to explore a possibility of 2D IR surface spectroscopy to detect intermolecular anharmonic couplings between CO and isotopic CO stretching modes on Cu(100) at different temperatures. In Sec. II details of the MD simulation are explained. The temperature dependence of the first-order response functions of IR spectroscopy and the second-order response functions of 2D IR surface spectroscopy are discussed in Sec. III and Sec. IV, respectively. Finally, concluding remarks are given in Sec. V.

## II. MOLECULAR DYNAMICS SIMULATION

In 2D Raman spectroscopy researchers have calculated the classical limit of the fifth-order Raman response function

$$R^{(5)}_{abcdef}(t_2,t_1) = -\frac{1}{kT}\langle \{\Pi_{ab}(t_2),\Pi_{cd}(0)\}_{\mathrm{PB}}\dot{\Pi}_{ef}(-t_1)\rangle, \quad (3)$$

where $\{\cdots\}_{\mathrm{PB}}$, $k$, and $T$ denote the Poisson bracket, Boltzmann constant, and temperature, respectively.[33–43] The response function [Eq. (3)] gives direct information on anharmonic dynamics[39,43] and coherent dynamics through the stability matrix.[39,40] Similarly, in 2D IR surface spectroscopy, it is necessary to calculate the classical limit of the second-order IR response function

$$R^{(2)}_{abc}(t_2,t_1) = -\frac{1}{kT}\langle \{\mu_a(t_2),\mu_b(0)\}_{\mathrm{PB}}\dot{\mu}_c(-t_1)\rangle$$
$$= -\frac{1}{kT}\left\langle \sum_{ij}\frac{\partial\mu_a(t_2)}{\partial q_i(t_2)}\frac{\partial q_i(t_2)}{\partial p_j(0)}\frac{\partial\mu_b(0)}{\partial q_j(0)}\dot{\mu}_c(-t_1)\right\rangle \quad (4)$$

in order to describe the surface dynamics and reveal the dynamical intermode correlation. We calculated the 2D surface IR signals by means of the MD simulation based on the stability matrix formalism, where calculation of stability matrix $\partial q_i(t_2)/\partial p_j(0)$ needs the $3N$ trajectories for one initial configuration, where $N$ is the number of particles. In this simulation, we set $abc=zzz$, where $z$ direction is vertical to the surface.

The following potentials were employed in our MD simulation; the Cu–Cu interaction potential developed by Wonchoba and Truhlar,[51] the Cu–C–O three-body potential and C–O intramolecular potential by Tully *et al.*[5] and the CO–CO interadsorbate potential by van der Pol *et al.*[52] and Janssen *et al.*[53] The interadsorbate potential included van der Waals terms and electronic terms representing dipole-dipole, dipole-quadrupole, and quadrupole-quadrupole interactions. The effects of e-h pair creation were included as stochastic forces and frictions whose parameters were made by Tully *et al.*[5] Similar MD simulations for CO on Cu surface have been performed to investigate the desorption of CO from Cu(100) enhanced by neighbor CO[54] and adsorption of CO on stepped surface of Cu(211).[55]

Our simulations were based on classical equations of motion for CO interacting with four surface layers with 16 Cu atoms in each layer. The bottom layer was rigid and interacted only with the nearest layer. Since the CO intramolecular force was much stronger than the other forces, we employed the multiple time scale MD (MTS-MD) algorithm[56] summarized in the Appendix. The time evolution was carried out for $t_1=t_2=1.6$ ps with $\Delta T=1$ fs and $\Delta t=0.1$ fs, where $\Delta T$ and $\Delta t$ are the longer and shorter time steps defined in the MTS method. $t_1=t_2=1.6$ ps is not enough to observe the linewidth of CO stretching mode in one-dimensional plots or 2D maps but is sufficient for the dynamical couplings between adsorbates. The Langevin equations were solved using Brunger-Brooks-Karplus algorithm.[57] To calculate the optical response, the dipole moment $\mu(t)$ was assumed to be

$$\mu(t) = \mu_0 + \mu_1 r(t), \quad (5)$$

where $\mu_0$ and $\mu_1$ denoted the permanent dipole moments and the first derivative of the dipole elements as the function of CO distance $r(t)$. By using GAUSSIAN 03, the parameters

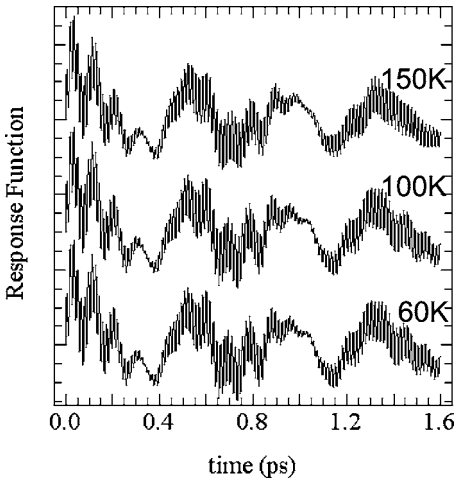


FIG. 2. Antisymmetric integrated response functions of second-order IR response functions at 60, 100, and 150 K. Curves are normalized at the maximum of the data.

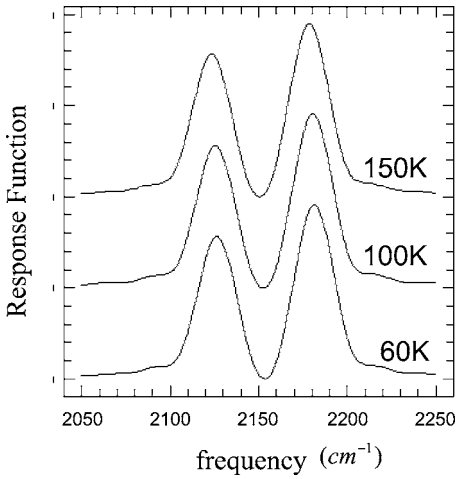


FIG. 3. Linear spectra at 60, 100, and 150 K. Curves are normalized as the area is the same at each temperature.

$\mu_0$=0.1326 Debye and $\mu_1$=9.098 Debye Å$^{-1}$ were determined from the optimized structure of free CO and OCCu with fixed 13 Cu atoms, respectively. The optimized geometries and dipole moments were calculated at the B3LYP/6-31G* level of the density functional theory (DFT).

The dipole moments for these high frequency modes are primarily determined by the intramolecular interactions. Therefore, the first derivatives of CO dipole moments with respect to Cu atom degrees of freedom are negligible compared with those with respect to C and O atoms, making it unnecessary to calculate the stability matrix of Cu atoms.

In 2D Raman spectroscopy of pure liquids, nonequilibrium MD (NEMD) simulations are computationally less expensive than MD simulations based on the stability matrix formalism.[36,42] This is because, for second-order IR or fifth-order Raman response functions, calculation of stability matrix requires $3N$ trajectories, while only four trajectories are needed in NEMD simulations.[42] However, when the simulations of multidimensional spectroscopy are directed to specific vibrational modes such as the CO vibrational mode of amide I in aqueous solution,[50] the above approximation requires only calculation of the stability matrix with respect to C and O atoms composing the CO vibrational mode and the atoms around them if needed. It should be stressed that the above approximation may make the MD simulations based on the stability matrix formalism computationally less expensive than the NEMD. Even though we neglected the stability matrices of Cu atoms, the present calculation included the motions of all atoms explicitly. This is different from the electrostatic DFT map method which separates the system from the bath and provides the entire fluctuating Hamiltonian including the effect of the bath.[58,59]

The 2D signals were calculated by averaging over 1 500 000, 1 200 000, and 700 000 initial configurations for 60, 100, and 150 K, respectively. Numerical convergence in time domain data was confirmed by checking the antisymmetric integrated response functions which characterized the behavior of stability matrix[40]

$$A(t,t) = 2\langle\mu(t)\{\mu(0),\mu(-t)\}_{\mathrm{PB}}\rangle - \langle\mu(0)\{\mu(0),\mu(-t)\}_{\mathrm{PB}}\rangle - \langle\{\mu(t),\mu(0)\}_{\mathrm{PB}}\mu(0)\rangle. \quad (6)$$

The antisymmetric integrated response functions for 60, 100, and 150 K are shown in Fig. 2.

## III. LINEAR RESPONSE FUNCTION

The MD simulations of the linear response functions were carried out for four CO's and isotopic CO's on Cu(100) at 60, 100, and 150 K. The spectra displayed in Fig. 3 show that the CO stretching frequencies of CO and isotopic CO were 2179 and 2123 cm$^{-1}$ at 150 K, respectively. The corresponding frequencies for one CO and isotopic CO on Cu(100) are 2175 and 2120 cm$^{-1}$. This shows blue shift due to the electronic interaction, in satisfactory agreement with the experiment.[6]

The spectra are independent of temperature in terms of the frequency. Indeed temperature has influence on the linewidth in the experiment, but the linewidth is not precisely reproduced in our simulation as stated in the previous section. Although the dynamics may be activated by increasing temperature, it has little effect on the CO stretching frequency. The spectra are not affected by the dynamics of neighbor adsorbates.

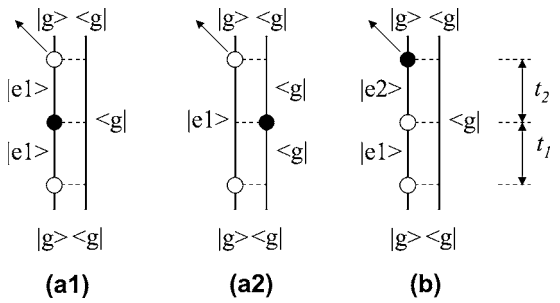


FIG. 4. Double-sided Feynman diagrams of 2D IR surface response function in CO on Cu(100) corresponding to the signals (a) in the fundamental tone area and (b) in the overtone area. $|g\rangle$, $|e1\rangle$, and $|e2\rangle$ represent ground state, one quantum excited states including $|1,0\rangle$ and $|0.1\rangle$, and two quanta excited states including $|2,0\rangle$, $|1,1\rangle$, and $|0,2\rangle$, respectively. White and black circles show once and twice interactions between laser field and system.

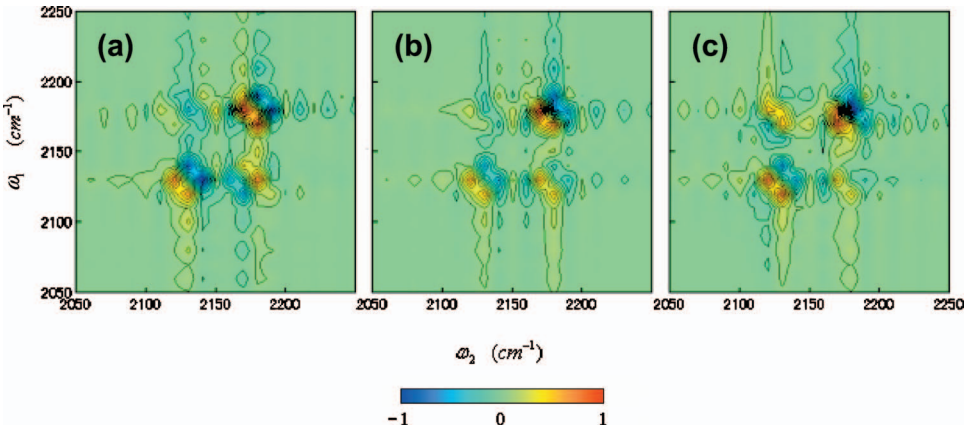


FIG. 5. (Color) Imaginary parts of 2D signals of the fundamental tone at (a) 60 K, (b) 100 K, and (c) 150 K. Spectra are normalized to have the same maximum.

## IV. TWO-DIMENSIONAL RESPONSE FUNCTION

One of the merits of the 2D techniques is their capacity to identify signals corresponding to specific Liouville space pathways.[19] Here, we focus only on CO stretching modes. The double-sided Feynman diagrams corresponding to the peaks on the areas of the fundamental tone area ($2050\ \mathrm{cm}^{-1} \leqslant \omega_1 \leqslant 2250\ \mathrm{cm}^{-1}$, $2050\ \mathrm{cm}^{-1} \leqslant \omega_2 \leqslant 2250\ \mathrm{cm}^{-1}$) and overtone area ($2050\ \mathrm{cm}^{-1} \leqslant \omega_1 \leqslant 2250\ \mathrm{cm}^{-1}$, $4100\ \mathrm{cm}^{-1} \leqslant \omega_2 \leqslant 4500\ \mathrm{cm}^{-1}$) are sketched in Figs. 4(a) and 4(b), respectively.[30]

The Fourier-transformed 2D signals, $\tilde{R}^{(2)}(\omega_2,\omega_1)$ in the fundamental tone area at different temperatures are depicted in Fig. 5. The main peaks are located at $(\omega_1,\omega_2)=(2123\ \mathrm{cm}^{-1},2123\ \mathrm{cm}^{-1})$, $(2123\ \mathrm{cm}^{-1},2179\ \mathrm{cm}^{-1})$, $(2179\ \mathrm{cm}^{-1},2123\ \mathrm{cm}^{-1})$, and $(2179\ \mathrm{cm}^{-1},2179\ \mathrm{cm}^{-1})$. Since the times $t_1=t_2=1.6$ ps are shorter than the relaxation time of signals, we observe weak sidelobe peaks along $\omega_1=2123,2179\ \mathrm{cm}^{-1}$ and $\omega_2=2123,\ 2179\ \mathrm{cm}^{-1}$.

The overtone transitions of a single oscillator such as $|0,0\rangle\langle 0,0| \rightarrow |2,0\rangle\langle 0,0|$ give larger contribution to the diagonal peaks than the transitions due to the interadsorbate couplings such as $|0,0\rangle\langle 0,0| \rightarrow |1,1\rangle\langle 0,0|$, where $|i,j\rangle$ represents the combination of $i$th excited state of CO and $j$th excited state of isotopic CO. Thus, the insensitivity of diagonal peaks to temperature indicates that the potential anharmonicity with respect to single CO stretching mode $g_{111} \equiv \partial^3 V/\partial r_1^3$ is unchanged. The volumes of the cross peaks in $|\tilde{R}^{(2)}(\omega_2,\omega_1)|^2$ are at most about one-tenth of those of the diagonal peaks.

The cross peaks representing anharmonic intermolecular couplings between CO and isotopic CO change significantly at 60, 100, and 150 K. The intermolecular couplings are caused by intermolecular anharmonic potentials composed by different CO stretch modes.[24] At least, three primary causes for interadsorbate couplings are possible; induced dipole moments on Cu surface (e-h pair creation), the couplings through surface Cu atoms (phonon effect), and electronic interactions between CO and isotopic CO. The first mechanism is excluded in our simulation because the effect of e-h pair creation is expressed by the frictions and stochastic forces[5] and cannot produce the correlation between CO and isotopic CO. Therefore, we consider the latter two possibilities. To examine the second mechanism, we calculated the 2D signal at 150 K by not allowing motion of the Cu atoms. The results shown in Fig. 6(a) resemble to Fig. 5(c), which indicates that the phonon effect is not dominant for interadsorbate couplings. To evaluate the third mechanism, we calculated the 2D map at 150 K with the electronic charges on CO to be zero and illustrated it in Fig. 6(b). The cross peaks at $(\omega_1,\omega_2)=(2123\ \mathrm{cm}^{-1},\ 2179\ \mathrm{cm}^{-1})$ in Fig. 6(b) are much weaker than those in Fig. 5, and the phase of the cross peaks at $(\omega_1,\omega_2)=(2179\ \mathrm{cm}^{-1},\ 2123\ \mathrm{cm}^{-1})$ also

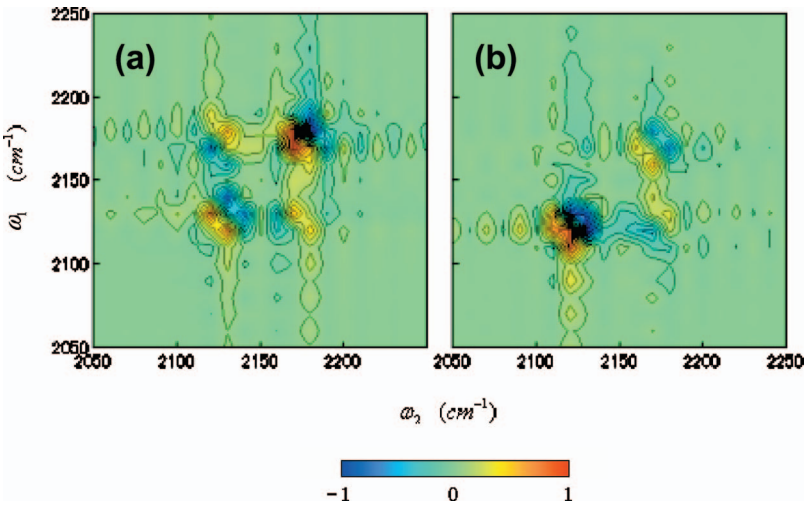


FIG. 6. (Color) Imaginary parts of 2D signals of the fundamental tone at 150 K (a) with Cu surface atoms fixed and (b) without electronic interactions.

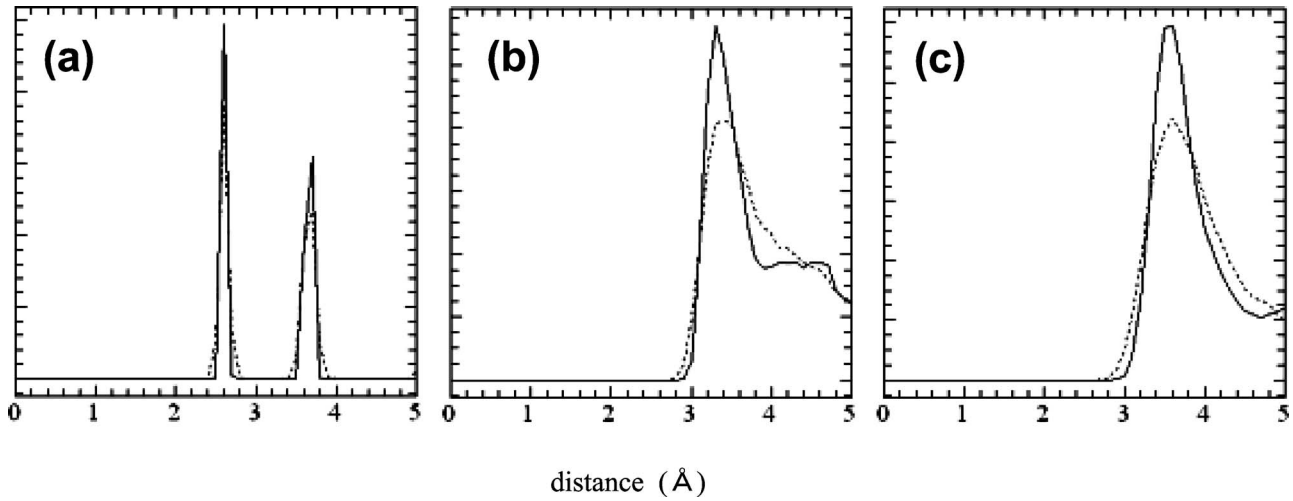


FIG. 7. Radial distribution functions of (a) Cu–Cu, (b) C–C, and (c) O–O at 60 K (solid) and 150 K (dotted).

changes between two figures. The interadsorbate interactions are primarily governed by electronic interactions which are about ten times stronger than van der Waals interactions. Therefore, the temperature dependence of the cross peaks may be attributed to electronic interactions.

Since the electric charges are fixed in our simulation, the electronic interaction strength depends on the distance between CO's. In Fig. 7, we show the radial distribution functions (RDFs) of C–C, O–O, and Cu–Cu. The C–C and O–O RDFs similarly expand with temperature in contrast to the Cu–Cu RDF, indicating that temperature activates the frustrated rotational mode. The nonlinear dipole moments and potential anharmonicities give nonvanishing elements in the second-order IR response function as in the fifth-order Raman response function.[32] The nonlinearity, however, plays a minor role on the second-order response function compared to the anharmonicity. In contrast, both give comparable contributions to the fifth-order Raman response function.[38,39,41,43] Based on these arguments, we focused mainly on the electronic interactions through the dynamics of CO and its potential anharmonicity. Our model is simplified to extract the lateral dipole-dipole couplings on surface; the electric charges $-q$ on adsorbates and $+q$ on metal surface are set and the angles between dipole moments and vertical line, $\theta_1$ and $\theta_2$, are selected as variables (Fig. 8). The interadsorbate potential of a right side adsorbate is given by

$$V = \frac{1}{4\pi\varepsilon}\frac{q^2}{((R - r_1 \sin\theta_1 + r_2 \sin\theta_2)^2 + (r_1 \cos\theta_1 - r_2 \cos\theta_2)^2)^{1/2}} - \frac{1}{4\pi\varepsilon}\frac{q^2}{((R + r_2 \sin\theta_2)^2 + (r_2 \cos\theta_2)^2)^{1/2}}, \tag{7}$$

where $R$ is the distance between surface atoms and $r_i$ is the distance between the $i$th adsorbate and the corresponding surface atom. The strengths of the cross peaks are proportional to the potential anharmonicity for different normal modes $g_{122} \equiv \partial^3 V / \partial r_1 \partial r_2^2$.[24,32,34] We plot $g_{122}$ in Fig. 9 as functions of $\theta_1$ and $\theta_2$ with $R = 3.6$ Å, $r_1 = r_2 = 1.9$ Å, and $r_1 q = 1$ Debye. Figure 9 shows that $g_{122}$ increases with $\theta_1 - \theta_2$. When $\theta_1 - \theta_2$ distribution for all adsorbates is obtained from our MD simulation (Fig. 10), we can observe that the rotational dynamics of adsorbates becomes active for higher temperature, which leads the wider $\theta_1 - \theta_2$ distribution. The wider $\theta_1 - \theta_2$ distribution increases the potential anharmonicity $g_{122}$ and changes the phase of the cross peaks, as seen in Fig. 9.

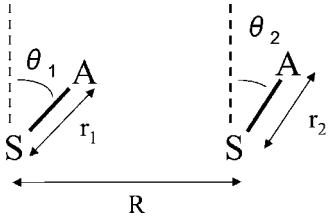


FIG. 8. The model with two dipole moments. A and S denote the adsorbate and surface atoms.

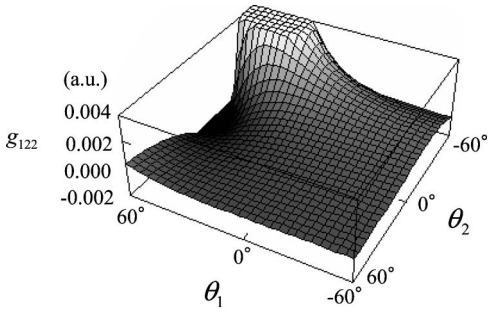


FIG. 9. Variation of anharmonicity $g_{122}$ with $\theta_1$ and $\theta_2$.

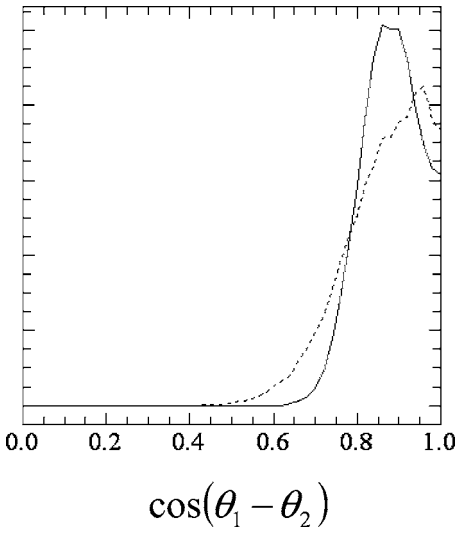


FIG. 10. $\cos(\theta_1-\theta_2)$ distribution at 60 K (solid) and 150 K (dotted) when Cu–Cu distance is less than 3.8 Å.

The calculated 2D signals in the overtone area at different temperatures are shown in Fig. 11. Comparing Fig. 5 with Fig. 11, we find that the cross peaks of Fig. 11 are much weaker than those of Fig. 5. This can be explained by the Feynman diagrams in Fig. 4. The cross peaks in the fundamental tone area arise from, for example, the optical process $|0,0\rangle\langle 0,0| \rightarrow |1,0\rangle\langle 0,0| \rightarrow |0,1\rangle\langle 0,0| \rightarrow |0,0\rangle\langle 0,0|$ in Fig. 4(a1). Similarly, the cross peaks in the overtone area arise from, for example, the process $|0,0\rangle\langle 0,0| \rightarrow |1,0\rangle\langle 0,0| \rightarrow |1,1\rangle\langle 0,0| \rightarrow |0,0\rangle\langle 0,0|$ in Fig. 4(b). The one quantum process $|1,0\rangle\langle 0,0| \rightarrow |1,1\rangle\langle 0,0|$ and two quanta processes, $|1,0\rangle\langle 0,0| \rightarrow |0,1\rangle\langle 0,0|$ and $|1,1\rangle\langle 0,0| \rightarrow |0,0\rangle\langle 0,0|$, require the couplings between CO and isotopic CO and have much less transition dipole moment than the one quantum processes, $|0,0\rangle\langle 0,0| \rightarrow |1,0\rangle\langle 0,0|$ and $|0,1\rangle\langle 0,0| \rightarrow |0,0\rangle\langle 0,0|$. Therefore the cross peaks in the fundamental tone area are stronger than those in the overtone area. Moreover, the diagonal peaks in the overtone area have opposite signs to the fundamental tone area. As was shown in the fifth-order Raman spectroscopy,[41] the peak intensities of the signals in frequency domain 2D maps are determined by the interplay between the nonlinear dipole moments (NL) and the anharmonicity of potentials (AN); NL+AN contributes to the diagonal peaks in the fundamental tone area, while NL-AN contributes to the diagonal peaks in the overtone area. Since the contributions of NL to 2D signals are much smaller than AN, the signs of the diagonal peaks in the fundamental tone and overtone areas are opposite according to the contributions of AN and −AN, respectively.

## V. CONCLUDING REMARKS

We have carried out the MD simulation for CO on Cu(100) to calculate the signals of 2D IR surface spectroscopy for various temperatures. Our MD simulation was based on the stability matrix formalism and the effect of e-h pair creation was expressed by the frictions and stochastic forces.[5] When temperatures were set to be 60, 100, and 150 K, the cross peaks were significantly changed in the fundamental tone areas of 2D frequency domain maps, while appreciable difference could not be found in linear response functions. Comparison of the signals from the MD simulations without electronic interactions and with surface Cu atoms fixed indicated that the electronic interactions were the primary cause of the temperature dependence of the cross peaks. To explore this point, we used a simple model with two dipole moments whose configurations were characterized by the angles between dipole moments and vertical line $\theta_1$ and $\theta_2$. We found that the increase of $\theta_1-\theta_2$ changed the potential anharmonicity due to the electronic interadsorbate interaction. In fact, wider $\theta_1-\theta_2$ distribution with temperature was observed in our simulation. The frustrated rotational mode activated by increasing temperature changed the anharmonicity of potentials and, consequently, the phases and intensities of cross peaks.

The cross peaks in the overtone area were much weaker than the fundamental tone area. This was because the former are second order in the couplings between CO and isotopic CO and the latter are first order. Moreover the phases of the diagonal peaks were changed between in the fundamental tone area and in the overtone area. This may be explained from our previous study of 2D Raman spectroscopy,[41] the anharmonicity of potentials with respect to the single CO stretching mode gave positive and negative contributions to the fundamental tone and the overtone, respectively.

Finally, we make the following two points. First, the e-h pair creation mechanism plays a major role in population decay on metal surface[2] and theoretical descriptions of e-h pair creation are well tested.[60] Although the effect of e-h pair

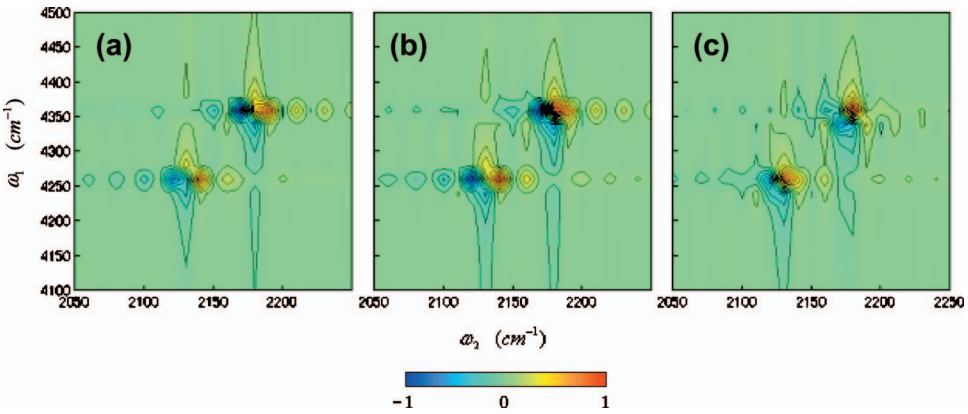


FIG. 11. (Color) Imaginary parts of 2D signals of the overtone at (a) 60 K, (b) 100 K, and (c) 150 K. All graphs are normalized to have the same maximum.

creation was treated by using the friction and stochastic forces in this study, it is challenging to simulate the influence of e-h pair creation on the inter-adsorbate couplings. Second, some studies have shown the capacity of 2D IR spectroscopy to investigate the intermolecular interactions by probing the intramolecular interactions.[61–64] For example, Zheng *et al.* probed the equilibrium dynamics of phenol complexation to benzene in a benzene-carbon tetrachloride solvent mixture,[61,62] and Cowan *et al.* investigated the loss of memory of persistent correlations in water structure.[63] In this study, the temperature dependence of the inter-adsorbate couplings was discussed by observing the cross peaks of the CO stretch. This study demonstrated the possibility of the multidimensional IR spectroscopies to detect the intermolecular couplings on surface as well as in bulk.

## ACKNOWLEDGMENTS

Y.N. is grateful to Professor E. O. Potma, Dr. T. Hayashi, Professor S. Saito, Y. Suzuki, Dr. H. Nakamura, Dr. K. Watanabe, Professor Y. Matsumoto, Dr. T. Yamada, and T. Hasegawa for fruitful discussions. Y.T. acknowledges the financial support from a Grant-in-Aid for Scientific Research A 15205005 from the Japan Society for the Promotion of Science. S.M. gratefully acknowledges the support of the Chemical Sciences, Geosciences and Biosciences Division, Office of Basic Sciences, U. S. Department of Energy. Some parts of the numerical calculation were performed at the Computer Center in the Institute of Molecular Science.

## APPENDIX: SUMMARY OF MTS-MD

The MTS method was introduced to lower the computation cost of integrating the equations of motion by separating all forces into short and long range types, $F_s$ and $F_l$.[56] These forces are integrated with different time steps. In one-dimensional system, the Liouville operator $L$ can be rewritten as

$$iL = iL_K + iL_{Vs} + iL_{Vl}, \tag{A1}$$

where

$$iL_K = \dot{x}\frac{\partial}{\partial x}, \tag{A2}$$

$$iL_{Vs} = F_s(x)\frac{\partial}{\partial p}, \tag{A3}$$

and

$$iL_{Vl} = F_l(x)\frac{\partial}{\partial p}. \tag{A4}$$

In the Verlet algorithm, the propagator can then be written as

$$e^{iL\Delta T} = e^{iL_{Vl}(\Delta T/2)}\left[e^{iL_K(\Delta t/2)}e^{iL_{Vs}\Delta t}e^{iL_K(\Delta t/2)} + O(\Delta t^3)\right]^n e^{iL_{Vl}(\Delta T/2)} + O(\Delta T^3), \tag{A5}$$

where $\Delta t = \Delta T/n$.

In our system, the force by the CO intramolecular potential corresponds to $F_s$, while all other forces are classified into $F_l$. The Liouville operator of the kinetic part can be decomposed into fast and slow motion parts corresponding to $F_s$ and $F_l$, respectively,

$$iL_K = iL_{Ks} + iL_{Kl}. \tag{A6}$$

Note that $L_{Ks}$ is dependent on the degrees of freedom of C and O atoms, while $L_{Kl}$ includes the degrees of freedom of all atoms. Since Cu atoms are independent of $F_s$, the time evolution of Cu atoms can be extracted from the iteration with smaller time step. Thus, we get

$$\begin{aligned} e^{iL\Delta T} &= e^{iL_{Vl}(\Delta T/2)}\left[e^{i(L_{Kl}+L_{Ks}+L_{Vs})\Delta t}\right]^n e^{iL_{Vl}(\Delta T/2)} + O(\Delta T^3) \\ &= e^{iL_{Vl}(\Delta T/2)}\left[e^{iL_{Ks}(\Delta t/2)}e^{iL_{Vs}\Delta t}e^{iL_{Ks}(\Delta t/2)} + O(\Delta t^3)\right]^n e^{iL_{Kl}\Delta T}e^{iL_{Vl}(\Delta T/2)} + O(\Delta T^3). \end{aligned} \tag{A7}$$

Equation (A7), avoiding $n$ times time evolution with respect to the position of Cu atoms, is compared with the original MTS-MD algorithm (A5).

The increase of the atoms independent of the short range forces accelerates the efficiency of Eq. (A7). The methodology is useful in the MD simulations ranging from the surface dynamics to the molecules in the solution in which the solute molecules are treated as rigid bodies and interact with the solute molecules. We explain it using the Verlet algorithm which is an example of a second-order symplectic integrator. This methodology is more important for the higher order symplectic integrator method.

[1] J. C. Tully, Annu. Rev. Phys. Chem. **51**, 153 (2000).
[2] B. N. J. Persson and M. Persson, Solid State Commun. **36**, 175 (1980); Y. Matsumoto and K. Watanabe, Chem. Rev. (Washington, D.C.) **106**, 4234 (2006).
[3] M. Head-Gordon and J. C. Tully, J. Chem. Phys. **96**, 3939 (1992).
[4] M. Head-Gordon and J. C. Tully, Phys. Rev. B **46**, 1853 (1992).
[5] J. C. Tully, M. Gomez, and M. Head-Gordon, J. Vac. Sci. Technol. A **11**, 1914 (1993).
[6] C. J. Hirschmugel, G. P. Williams, F. M. Hoffmann, and Y. J. Chabal, Phys. Rev. Lett. **65**, 480 (1990).
[7] C. J. Hirschmugel and G. P. Williams, Phys. Rev. B **52**, 14177 (1995).
[8] J. P. Culver, M. Li, L. G. Jahn, R. M. Hochsrasser, and A. G. Todh, Chem. Phys. Lett. **214**, 431 (1993).
[9] T. A. Germer, J. C. Stephenson, E. J. Heilweil, and R. R. Cavanagh, J. Chem. Phys. **101**, 1704 (1994).
[10] A. P. Graham, F. Hofmann, J. P. Toennies, G. P. Williams, C. J. Hirschmugl, and J. Ellis, J. Chem. Phys. **108**, 7825 (1998).
[11] H. Kato, M. Kawai, and J. Yoshinobu, Phys. Rev. Lett. **82**, 1899 (1999).
[12] J. Yoshinobu, N. Takagi, and M. Kawai, Phys. Rev. B **49**, 16670 (1994).
[13] H. J. Lee and W. Ho, Science **286**, 1719 (1999).
[14] T. Komeda, Y. Kim, M. Kawai, B. N. J. Persson, and H. Ueba, Science **295**, 2055 (2002).
[15] L. Bartels, F. Wang, D. Moller, E. Knoesel, and T. F. Heinz, Science **305**, 648 (2004).
[16] E. Borguet and H. L. Dai, J. Phys. Chem. B **109**, 8509 (2005).
[17] P. Jakob, Phys. Rev. Lett. **77**, 4229 (1996).
[18] P. Jakob and B. N. J. Persson, J. Chem. Phys. **109**, 8641 (1998).
[19] S. Mukamel, *Principles of Nonlinear Optical Spectroscopy* (Oxford University Press, New York, 1995).
[20] Y. Tanimura and S. Mukamel, J. Chem. Phys. **99**, 9496 (1993).
[21] Y. R. Shen, *The Principles of Nonlinear Optics* (Wiley-Interscience, New York, 1984).
[22] Y. R. Shen, Nature (London) **337**, 519 (1989).
[23] P. Guyot-Sionnest, Phys. Rev. Lett. **66**, 1489 (1991).
[24] M. Cho, Phys. Rev. A **61**, 023406 (2000).
[25] M. Bonn, C. Hess, J. H. Miners, T. F. Heinz, H. J. Bakker, and M. Cho, Phys. Rev. Lett. **86**, 1566 (2001).
[26] M. H. Cho, C. Hess, and M. Bonn, Phys. Rev. B **65**, 205423 (2002).
[27] N. Belabas and M. Joffre, Opt. Lett. **27**, 2043 (2002).

[28] C. Voelkmann, M. Reichelt, T. Meier, S. W. Koch, and U. Hofer, Phys. Rev. Lett. **92**, 127405 (2004).
[29] M. Cho, J. Chem. Phys. **112**, 9978 (2000).
[30] K. Okumura and Y. Tanimura, J. Phys. Chem. A **107**, 8092 (2003).
[31] R. Venkatramani and S. Mukamel, J. Phys. Chem. B **109**, 8132 (2005).
[32] K. Okumura and Y. Tanimura, J. Chem. Phys. **107**, 2267 (1997).
[33] S. Mukamel, V. Khidekel, and V. Chernyak, Phys. Rev. E **53**, R1 (1996).
[34] S. Saito and I. Ohmine, J. Chem. Phys. **108**, 240 (1998).
[35] A. Ma and R. M. Stratt, Phys. Rev. Lett. **85**, 1004 (2000).
[36] T. l. C. Jansen, J. G. Snijders, and K. Duppen, J. Chem. Phys. **113**, 307 (2000).
[37] S. Saito and I. Ohmine, Phys. Rev. Lett. **88**, 207401 (2002).
[38] A. Ma and R. M. Stratt, J. Chem. Phys. **116**, 4972 (2002).
[39] S. Saito and I. Ohmine, J. Chem. Phys. **119**, 9073 (2003).
[40] Y. Nagata and Y. Tanimura, J. Chem. Phys. **124**, 024508 (2006).
[41] Y. Nagata, T. Hasegawa, and Y. Tanimura, J. Chem. Phys. **124**, 194504 (2006).
[42] T. Hasegawa and Y. Tanimura, J. Chem. Phys. **125**, 074512 (2006).
[43] S. Saito and I. Ohime, J. Chem. Phys. **125**, 084506 (2006).
[44] R. DeVane, C. Ridley, B. Space, and T. Keyes, J. Chem. Phys. **119**, 6073 (2003).
[45] S. Woutersen and P. Hamm, J. Chem. Phys. **114**, 2727 (2001).
[46] J. Bredenbeck and P. Hamm, J. Chem. Phys. **119**, 1569 (2003).
[47] C. Fang, J. Wang, A. K. Charnley, W. Barber-Armstrong, A. B. Smith, S. M. Decatur, and R. M. Hochstrasser, Chem. Phys. Lett. **382**, 586 (2003).
[48] P. Mukherjee, A. T. Krummel, E. C. Fulmer, I. Kass, I. T. Arkin, and M. T. Zanni, J. Chem. Phys. **120**, 10215 (2004).
[49] C. Fang, J. Wang, Y. S. Kim, A. K. Charnley, W. Barber-Armstrong, A. B. Smith, S. M. Decatur, and R. M. Hochstrasser, J. Phys. Chem. B **108**, 10415 (2004).
[50] Y. S. Kim, J. Wang, and R. M. Hochstrasser, J. Phys. Chem. B **109**, 7511 (2005).
[51] S. E. Wonchoba and D. G. Truhlar, J. Chem. Phys. **99**, 9637 (1993).
[52] A. van der Pol, A. van der Avoird, and P. E. S. Wormer, J. Chem. Phys. **92**, 7498 (1990).
[53] W. B. J. M. Janssen, J. Michiels, and A. van der Avoird, J. Chem. Phys. **94**, 8402 (1991).
[54] C. Springer and M. Head-Gordon, Chem. Phys. **205**, 73 (1996).
[55] M.-C. Marinica, H. Le Rouzo, and G. Raseev, Surf. Sci. **542**, 1 (2003).
[56] M. Tuckerman, B. J. Berne, and G. J. Martyna, J. Chem. Phys. **97**, 1990 (1992).
[57] A. Brunger, C. L. Brooks, and M. Karplus, Chem. Phys. Lett. **105**, 495 (1984).
[58] T. Hayashi, T. l. C. Jansen, W. Zhuang, and S. Mukamel, J. Phys. Chem. A **109**, 64 (2005).
[59] T. Hayashi, W. Zhuang, and S. Mukamel, J. Phys. Chem. A **109**, 9747 (2005).
[60] H. Nakamura and K. Yamashita, J. Chem. Phys. **122**, 194706 (2005).
[61] J. R. Zheng, K. Kwak, J. Asbury, Z. Chen, I. R. Pilectic, and M. D. Fayer, Science **309**, 1338 (2005).
[62] K. Kwak, C. Lee, Y. Jung, J. Han, K. Kwak, J. R. Zheng, M. D. Fayer, and M. Cho, J. Chem. Phys. **125**, 244508 (2005).
[63] M. L. Cowan, B. D. Bruner, N. Huse, J. R. Dwyer, B. Chung, E. T. J. Nibbering, T. Elsaesser, and R. J. D. Miller, Nature (London) **434**, 199 (2005).
[64] J. D. Eaves, J. J. Loparo, C. J. Fecko, S. T. Roberts, A. Tokmakoff, and P. L. Geissler, Proc. Natl. Acad. Sci. U.S.A. **102**, 13019 (2005).